Observing system simulation experiments with ensemble Kalman filters in Nantucket Sound, Massachusetts

Pengfei Xue,[1] Changsheng Chen,[1,2,3] Robert C. Beardsley,[1,2] and Richard Limeburner[2]

[1]   Observing system simulation experiments (OSSEs) were performed for Nantucket Sound, Massachusetts, as a pilot study for the design of optimal monitoring networks in the coastal ocean. Experiments were carried out using the ensemble Kalman filter (EnKF) for data assimilation with ensemble transform Kalman filter (EnTKF) and proper orthogonal decomposition (POD) for selecting the optimal monitoring sites. The singular evolutive interpolated Kalman filter (SEIK) was compared with EnKF for the data assimilation efficiency. Running the unstructured grid Finite-Volume Community Ocean Model (FVCOM) with perturbed initial fields of currents, water temperature, and salinity show that in this shallow coastal system, the velocity and surface elevation are able to restore themselves back to the true state over an inertial time scale after perturbation without data assimilation, while the water temperature and salinity are not. This suggests that in this vertically well mixed region with strong tidal influence, monitoring should be targeted at water properties rather than velocities. By placing measurement sites at an entrance or exit or a location with the maximum signal variance (EnTKF) or at extrema of the dominant EOF spatial modes (POD), we evaluated the capability of EnTKF and POD in designing the optimal monitoring site for the forecast model system in this region. The results suggest that understanding the multiscale dynamical nature of the system is essential in designing an optimal monitoring network since "optimal" sites suggested by an assimilation method may only represent a local-scale feature that has little influence on a region-wide system. Comparing EnKF and SEIK simulations shows that SEIK can significantly improve the data assimilation efficiency by reducing the ensemble number and increasing the convergence rate.

Citation: Xue, P., C. Chen, R. C. Beardsley, and R. Limeburner (2011), Observing system simulation experiments with ensemble Kalman filters in Nantucket Sound, Massachusetts, *J. Geophys. Res.*, *116*, C01011, doi:10.1029/2010JC006428.

1. Introduction

[2] Integrated ocean observation systems (IOOS) have received extensive public and government attention, with an aim at predicting the response of coastal ecosystems to global climate change; improving the safety and efficiency of maritime operations; mitigating the damages from natural and environmental hazards; and maintaining ocean and coastal resources [*Intergovernmental Oceanographic Commission*, 2003]. By efficiently linking between monitoring network, modeling and management, an IOOS can form an "end-to-end" system with forecast capability. Building and maintaining an observational network, however, is extremely costly, so that an optimal design of this

system is a key issue that directly affects whether or not an IOOS will succeed. Observing system simulation experiments (OSSEs), which were used by *Charney et al.* [1969] for the Global Atmospheric Research Program (GARP), have been adopted for the design of an observing system aimed to improve ocean prediction through the use of data assimilation [*Hackert et al.*, 1998; *Raicich and Rampazzo*, 2003; *Ballabrera-Poy et al.*, 2007].

[3] As a modeling component of the Northeast Regional Association of Coastal Ocean Observing Systems (NERACOOS), a joint research team of University of Massachusetts Dartmouth and Woods Hole Oceanographic Institution has developed the Northeast Coastal Ocean Forecast System (NECOFS). Nantucket Sound was selected as a pilot OSSE site by the Massachusetts Institute of Technology Sea Grant Program for the design of an optimal monitoring network in Massachusetts (Figure 1). Bounded by Cape Cod on the north, Nantucket Island and Martha's Vineyard Island on the south, Nantucket Sound is a tidally dominated, "flow-through" system that connects Cape Cod inlets, bays, and estuaries to adjoining "upstream" waters (the Gulf of Maine to the east and the New England shelf to the

[1]School for Marine Science and Technology, University of Massachusetts Dartmouth, New Bedford, Massachusetts, USA.
[2]Department of Physical Oceanography, Woods Hole Oceanographic Institution, Woods Hole, Massachusetts, USA.
[3]Marine Ecosystem and Environment Laboratory, College of Marine Science, Shanghai Ocean University, Shanghai, China.
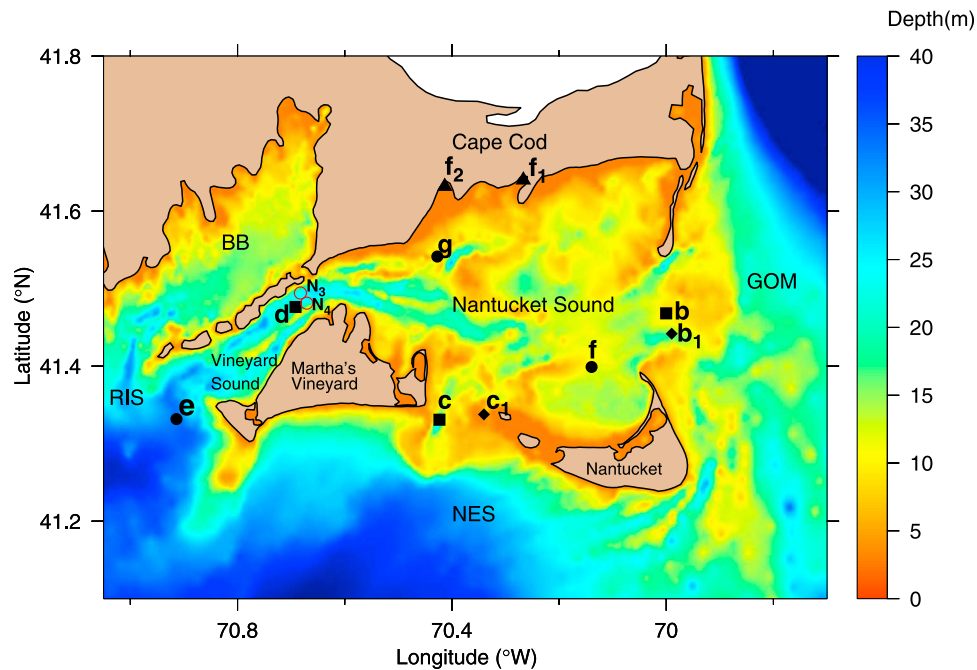
Figure 1. Bathymetry of Nantucket Sound and adjacent region. Letters b–g denote sampling locations selected for experiments (see text). The site marked "e" is the maximum signal variance site predicted by EnTKF. Sites f, f_1, and f_2 are optimal sampling sites suggested by the first mode of POD analysis using the temperature fields of the initial ensemble, hourly model output of the first week in June, and 3-hourly model output over June, respectively. The site marked "g" is the maximum $\bar{S}$ site suggested by the coherence analysis method on the basis of the forecast error covariance. Red circles are the Nobska moorings (N_3 and N_4) deployed in 2006 to measure cross-channel structure of the Vineyard Sound current. Nantucket Sound borders the Gulf of Maine (GOM) to the east and the New England Shelf (NES) to the south and through Vineyard Sound to the west with Rhode Island Sound (RIS) and Buzzards Bay (BB).

south) and "downstream" waters (Vineyard Sound and Buzzards Bay). Due to strong tidal flushing around islands and significant temporal variation in wind forcing, currents in Nantucket Sound are characterized by complex geometrically controlled multiscale variability.

[4] The Nantucket Sound component of NECOFS was validated through a comparison of modeled and observed tidal and subtidal currents, water temperature and salinity for 2004–2006; an example for the 2006 subtidal current comparison is presented in Figure 2. With resolution of the complex coastal geometry, the model captures both spatial and temporal variability of currents and stratification in Nantucket Sound. The accuracy of the model simulations provides a foundation to be used for OSSEs.

[5] The primary objective of the OSSEs in Nantucket Sound is to use data assimilation methods to help in the design of an optimal field measurement plan for the forecast model system in this coastal area. As a sister project, *Yang et al.* [2011] used the proper orthogonal decomposition (POD) based approach to select optimal sensor locations in Nantucket Sound. As an alternative approach, we have adopted the ensemble Kalman filter methods. By conducting twin experiments with an ensemble of initial perturbed fields generated using a Monte Carlo approach [*Evensen*, 1994], we have examined the dependence of the success of data assimilation on memory of the local dynamics system, the

impact of ensemble size on the success of OSSE-based data assimilation experiments, and the optimal design of monitoring sites in this area. A comparison is also made on Kalman filter and POD methods based on a dynamical analysis of the flow characteristics in Nantucket Sound.

[6] This paper summarizes the OSSEs results in Nantucket Sound. In section 2, the hydrodynamic model and design of the data assimilation experiments are described. In section 3, the nature of self-restoration of momentum in Nantucket Sound is explored. In section 4, the results of different experiments are presented. In section 5, comparisons of different optimal sampling strategies are conducted and discussed. In section 6, Lagrangian particles and tracer-tracking experiments are made to understand the influence of the local multiscale dynamics on the data assimilation performance. Conclusions are summarized in section 7. EnKF and SEIK are compared regarding ensemble size and computational efficiency in Appendix A.

2. The Model, Data Assimilation Methods, and Design of the Experiments

2.1. The Model and Study Site

[7] The OSSEs in Nantucket Sound were conducted using the second-generation Gulf of Maine FVCOM (hereafter referred to as FVCOM-GOM2): the unstructured
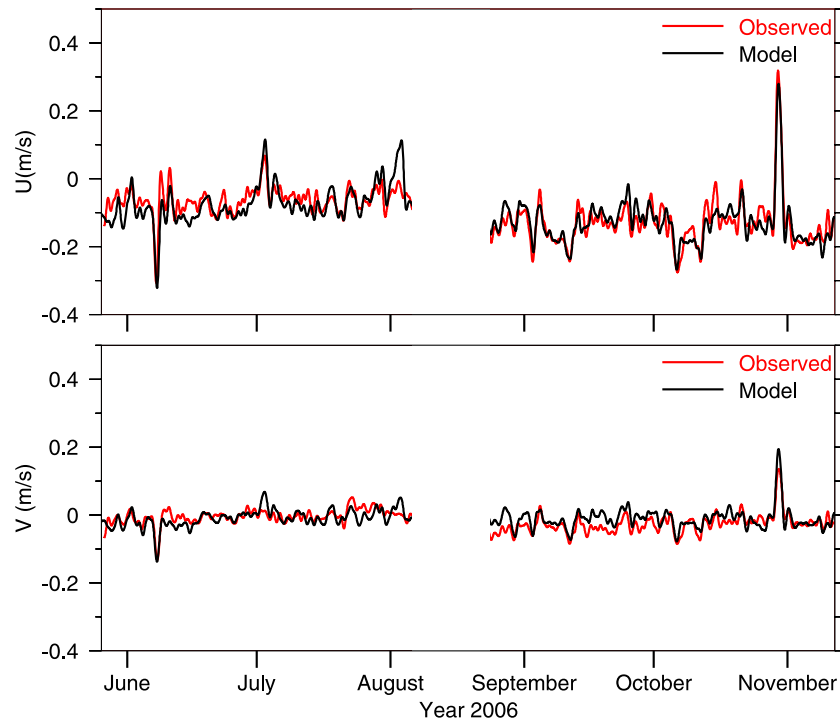
Figure 2. Comparison between the observed (red) and simulated (black) subtidal surface currents at mooring sites (N_3 and N_4) in the west exit of Vineyard Sound. The buoy N_3 was located at 41° 29.669′N, 70°40.961′W in May–August 2006 and then moved to N_4 at 41°28.870′N, 70°40.251′W in September–November 2006.

grid, finite volume, three-dimensional (3D) primitive equation coastal ocean model configured as the ocean model component of NECOFS (http://fvcom.smast.umassd. edu/research_projects/NECOFS/index.html) for the Gulf of Maine and New England coastal ocean [*Chen et al.*, 2003, 2006a, 2006b]. FVCOM-GOM2 uses the generalized terrain-following coordinate system [*Pietrzak et al.*, 2002] in the vertical and nonoverlapping triangular meshes in the horizontal. The flux formulation for momentum and scalars (e.g., temperature, salinity) are solved numerically using the second-order accurate finite volume scheme, which guarantees mass conservation in both local individual cells and the entire domain. FVCOM-GOM2 has been validated by hindcast simulation of tidal and subtidal currents, temperature and salinity, and an example for Nantucket Sound is presented in Figure 2.

[8] The twin data assimilation experiments in Nantucket Sound were conducted in the NECOFS subdomain area shown in Figure 3. This subdomain is linked to FVCOM-GOM2 through a one-way nesting approach, with the horizontal resolution varying from 0.3 to 0.5 km inside Nantucket Sound to 9 km off the coast to the open boundary. In the vertical, the water column is divided into 30 layers, with a resolution of ~0.3 m or less inside Nantucket Sound. The model was driven by tidal forcing, surface wind stress and atmospheric pressure, surface heat flux, net precipitation minus evaporation, plus freshwater discharge from the coastal rivers. FVCOM-GOM2 was solved using the mode–split time integration approach, with time steps of 4.0 s for the external mode and 40 s for the internal mode.

2.2. Data Assimilation Methods

[9] The OSSEs were carried out using ensemble Kalman filter (EnKF) [*Evensen*, 2003, 2004; *Chen et al.*, 2009] for data assimilation, with options of the ensemble transform Kalman filter (EnTKF) [*Bishop et al.*, 2001; *Majumdar et al.*, 2002] and proper orthogonal decomposition (POD) [*Yang et al.*, 2011] for selecting the optimal monitoring sites. The singular evolutive interpolated Kalman filter (SEIK) [*Pham et al.*, 1998; *Pham*, 2001] was used to compare EnKF for the data assimilation efficiency. To shorten the text, the discussion of the EnKF and SEIK comparison is described in Appendix A.

[10] EnKF can be derived from the traditional analysis equation in the Kalman filter in the form of

$$x^a = x^f - K(y - Hx^f), P^a = P^f - KHP^f,$$
$$K = P^f H^T (HP^f H^T + R)^{-1} \tag{1}$$

where x^f and x^a denote arrays of model forecast and analysis values, respectively; y is an array of observational values; K is the Kalman gain, P^f, P^a and R are the forecast, analysis and observational error covariances, respectively; and H is an observational operator that functions as an objective map to interpolate the model data onto the observational points. EnKF is a Monte Carlo approximation of the Kalman filter, which essentially replaces error covariance matrix by the sample covariance from ensemble states. Given an ensemble of model forecast states x_j^f (j = 1, 2, 3,…, n_e) with size n_e, EnKF calculates (1) for each member of the ensemble and
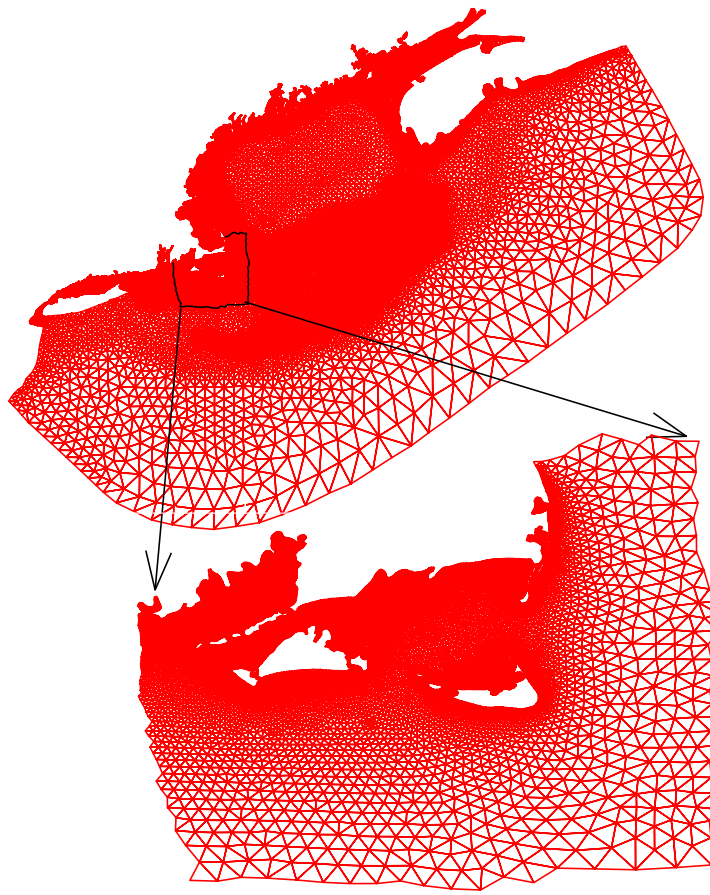
Figure 3. Unstructured grid of (bottom) FVCOM-NS nested with (top) the second-generation regional model FVCOM-GOM2. The black line shown in the top grid is the location of the node at the nesting boundary. See http://fvcom.smast.umassd.edu/research_projects/NECOFS/index.html for more information about NECOFS and FVCOM-GOM2.

updates the model field using the ensemble mean of analysis values. In practice, an ensemble of initial perturbed fields is generated by randomly selecting snapshots of model simulation results using a Monte Carlo approach.

[11] EnTKF can also be derived from the traditional analysis equation in the Kalman filter described in (1). The transformation matrix $\hat{T}$ is defined by

$$\hat{T} = C(\Gamma + I)^{-1/2} \tag{2}$$

where C and Γ are eigenvectors and eigenvalues of the matrix $x_f^T H^T R^{-1} H x_f$. With this transformation, the analysis error covariance equation in (1) can be rewritten as

$$P^a = P^f - x_f \left[C\Gamma(1 + \Gamma)^{-1} C \right] x_f^T \tag{3}$$

where $x_f = (x^f - \bar{x}^f) / \sqrt{n_e - 1}$. The overbar represents the ensemble mean. Using (3), one can explicitly estimate the prediction and analysis error variances. An optimal monitoring site can be determined by selecting a location at which the trace of P^a reaches its minimum. This is equivalent to selecting a location at which the signal variance defined by the trace of the second term on the right side of (3) reaches its maximum. In fact, for small models, it might be feasible to simply compute $P^f H^T (HP^f H^T + R)^{-1} HP^f$ in equation (1) and its trace for all possible observational networks H to find that which minimizes analysis error variance, but EnTKF provides a more computationally efficient way to estimate the analysis error variance and even its propagation to future forecasts. In practice, it is achieved by running EnTKF experiments by selecting computational nodes or cells to determine the site for maximum signal variance. This approach was first recommended by *Bishop et al.* [2001] for atmospheric data assimilation experiments and tested by S. J. Lyu et al. (Optimal fixed and adaptive observation arrays in an idealized wind-driven ocean model, unpublished manuscript, 2009) to design optimal fixed and adaptive observation arrays in an idealized wind-driven ocean model. The same approach was used in our EnTKF experiments.

[12] POD is principally an EOF analysis method. Let $V(t)$ be the true state variables. By using EOF analysis, $V(t)$ can be approximated by

$$V(t) \approx \tilde{V}(t) = \sum_{i=1}^{K} b_i(t)\varphi_i \qquad (4)$$

where $\tilde{V}(t)$ is the analysis state variables, φ_i is the ith dominant EOF mode, $b_i(t)$ is the corresponding coefficient of φ_i, and K is the number of significant EOF modes. The best prediction can be reached for the condition

$$E = \| V(t) - \tilde{V}(t) \|_m^2 \Rightarrow \min \qquad (5)$$

where m is called the mask vector, which only counts the variable value at observational sites. Substituting (4) into (5) and differentiating (5) with respect to $b_i(t)$, we can derive a linear algebra matrix in the form of

$$Mb = l \qquad (6)$$

where M is a matrix consisting of $(\varphi_i, \varphi_i)_m$ and l the vector array constructed by $(V_m(t), \varphi_i)_m$., where $V_m(t)$ is the point-wise product of the mask vector m and $V(t)$.

[13] In an incomplete (gappy) true state system, the true value of $V(t)$ in (4) is only known at measurement sites but unknown at all other locations. Different designs of measurement strategy produce different M. Based on the requirement for minimum E, *Willcox* [2006] suggested that sampling should be taken for the condition in which M has a minimal matrix condition number (defined as the ratio of the maximum singular value to the minimum singular value of the matrix M). *Yildirim et al.* [2009] pointed out in their experiments that this approach does not always work well. Instead, they proposed placing the observational sites at locations where the variations of the dominant EOF modes are the largest. Recently, *Yang et al.* [2011] found that in Nantucket Sound, the largest variation points of different EOF modes may be very close to each other. Eliminating these close points could help reduce the number of the observational sites and thus improve the efficiency of the optimal design. In our experiments, we did not repeat the work of *Yang et al.* [2011]. Instead, we used their POD ideas to select observational site(s) at the largest variation points of the dominant EOF modes and run the model using EnKF to compare the results with other methods.

[14] Combining the advantages of POD and EnTKF methods, we developed a new method to determine the optimal observational locations using the coherence function constructed by the forecast error covariance. Following EnTKF, we first calculate the correlation matrix D as

$$D_{i,j} = \frac{P_{i,j}}{\sqrt{P_{i,i}}\sqrt{P_{j,j}}} \qquad (7)$$

where $D_{i,j}$ and $P_{i,j}$ are the ith row and jth column of D and P^f, respectively. Considering the observation sites, we define S as the sum of all elements of HD (here H is the observation operator defined in EnKF) in the form of

$$S = \sum (HD)_{i,j} \qquad (8)$$

where $(HD)_{i,j}$ is the ith row and jth column of HD, H will differ as the observation site changes. The optimal observational site can be determined by selecting a point at which S has its maximum. This is also equivalent to selecting a point at which the maximum value of $\bar{S}$(mean of S) is found.

2.3. Experiment Designs

[15] The OSSEs were made through twin experiments in which the hindcast model simulation is defined as the "nature" run and served as the true state of the OSSE to compare with the assimilation model run with perturbed initial conditions. The data assimilation is approached by selecting hourly sampled time series of the data at "monitoring sites" from the hindcast model simulation and adding the random noise at a scale of 0.01°C to represent observational errors. The convergence of the assimilation run toward the true state is used to measure the success and efficiency of the data assimilation method. The comparison of the assimilation model runs with different monitoring sites provides us with a view of the sensitivity of the model convergence rate to selection of observational sites and variables and thus helps us design an optimal local observational system to meet the requirement for the short- and long-term forecast capability of a model.

[16] Four twin experiments were conducted for the summertime period of 1–30 June 2006. This is the period with the largest spatial variation of water temperature, even though the water is vertically well mixed. Experiment 1 (Ex1) was designed to examine the memory of currents and water properties to the initial perturbation. The primary question was whether or not the flow and water property fields could restore back to the true solution after the initial perturbation if the external forcing and boundary conditions were correct. This experiment was made by running the nested Nantucket Sound subdomain model with incorrect initial fields of flow, temperature and salinity without data assimilation. Experiment 2 (Ex2) was made to examine the capability of EnKF to filter the initial noise and restore the model fields toward the true solution by assimilating the data at monitoring sites at the entrance or exit boundaries of Nantucket Sound. Experiment 3 (Ex3) was aimed at comparing different optimal sampling model techniques on the performance of the design of the optimal observing system. These techniques included the choice of the monitoring sites by seeking (1) the maximum signal variance (Sig-Var) suggested by EnTKF [*Bishop et al.*, 2001], (2) the maximum variance of EOF spatial modes suggested by POD [*Willcox*, 2006; *Yildirim et al.*, 2009; *Yang et al.*, 2011], and (3) the maximum correlation area between the monitoring site and the entire assimilation domain (hereafter referred to as Max-Corr). Experiment 4 (Ex4) was conducted to compare the EnKF and SEIK methods. The size of the ensemble is a critical issue that can limit the use of EnKF in realistic forecast applications. We hypothesize that the ensemble size should be determined by the physical dynamics in the study region, which can be better understood with EOF analysis. If this approach is correct, SEIK, with initial ensemble members constructed using the dominant modes of EOF, should work efficiently in coastal applications. Ex4 was designed to answer this question. The EnKF data assimilation was approached using an ensemble with twenty members suggested for coastal ocean problems by *Chen et al.* [2009], and
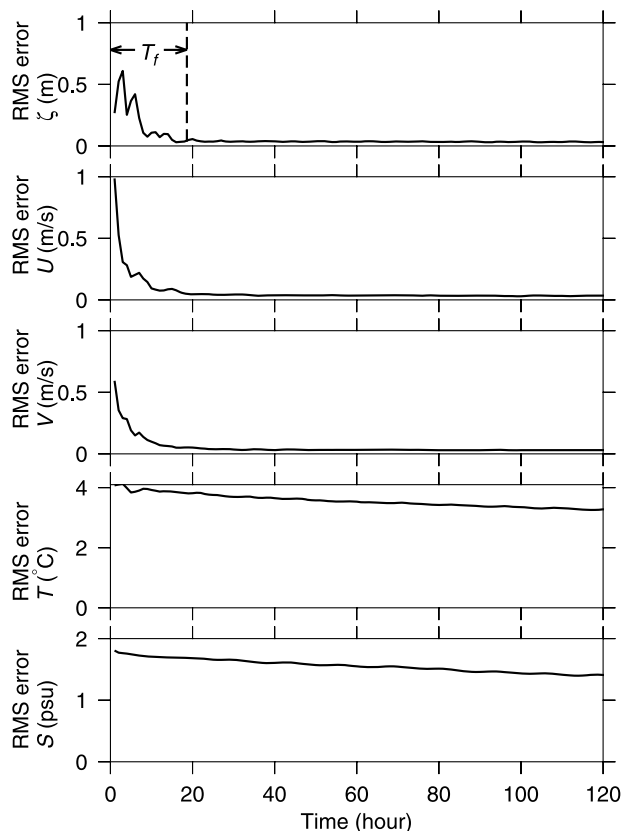
Figure 4. Change of the domain-averaged RMS errors in surface elevation, currents, temperature, and salinity with time after the initial perturbation for the case (case a) without assimilation. The inertial period (T_f) is 18.62 h in Nantucket Sound.

the ensemble of initial perturbed fields was generated by randomly selecting daily snapshot of model simulation results in the previous month. Whether or not twenty members were sufficient is discussed in Ex4.

[17] To help understand the performance of different data assimilation methods in the selection of different monitoring sites, we have examined the dynamics controlling the dominant physical processes in this system. Tracking Lagrangian particles and releasing dye tracers provide a detailed description of the temporal and spatial scale of water movement in Nantucket Sound. Our study suggests that in addition to simply relying on existing data assimilation technology, understanding the multiscale nature of the local dynamical system is helpful in the design of the optimal sampling plan.

3. Self-Restoring Nature of Momentum in NS

[18] Data assimilation is aimed to restore the system toward its true solution. However, it would become unnecessary if the system is capable of restoring itself after initial perturbation. For the tidal flushing case in an idealized estuary, *Chen et al.* [2009] found that the data assimilation becomes trivial and the model field in such a highly dissipative estuarine system can converge rapidly toward the true state without any assimilation. Nantucket Sound is a

vertically well mixed region characterized by strong tidal flushing. The first question here is whether this region is a self-restoring system.

[19] Ex1 shows that without data assimilation, the surface elevation and currents converge toward the true state in a short time scale of ~19 h, while the temperature and salinity fields contain large errors over a much longer time scale (Figure 4). These features remain similar no matter how the initial fields of currents and water properties are perturbed. The inertial period in Nantucket Sound is 18.6 h. This experiment indicates that currents in Nantucket Sound have a short memory to its initial condition. For given correct surface forcing and boundary conditions, it can self-restore toward its true states over an inertial time period without using data assimilation.

[20] The fact that the temperature and salinity fail to restore toward the true solution in Ex1 suggests that the response of scalar variables to initial perturbation differs from the momentum. The scalar tracers have a long memory of their initial condition, so that once their initial condition is destroyed, it would take a much longer time to adjust back to the true solution. This can be explained using a simple box model for water temperature. In this experiment, the change of the mean temperature in the nested Nantucket Sound subdomain is controlled by surface heating and flux from the lateral boundaries such as

$$\bar{T} = \bar{T}_o + \frac{\Delta t}{\rho c_p V}\left(Q_{surface} + Q_{boundaries}\right) \qquad (9)$$

where T is water temperature, the overbar indicates the mean value over the total water volume (V), subscript o represents the initial state, c_p is the specific heat capacity, ρ is the density of seawater, $Q_{surface}$ and $Q_{boundary}$ are the surface and lateral boundary heat fluxes, and Δt is the time interval. For given surface and lateral boundary heat fluxes, equation (9) shows that the mean temperature in this region depends on the value of $\bar{T}_o$. The surface and lateral heat fluxes contribute to the change of the temperature, but the mean temperature in the region depends on the initial condition. Once the initial condition is destroyed, the system would not be able to restore back without the aid of data assimilation. The role of data assimilation is to add or subtract heat into the system. This result is also applicable for salinity.

[21] We have learned from Ex1 that in this vertically well mixed region, if the surface and boundary forcing are correct, the momentum has a self-restoration nature over an inertial time period, while the water mass cannot restore over such a short time period. Once the water mass is perturbed from its true state, the model fails to converge toward the true solution without data assimilation.

4. The EnKF Experiment Results

[22] Nantucket Sound is a "flow through" dynamical system. One straightforward design is to set up the monitoring sites at the entrance or exit of this system. Ex2 was designed to use EnKF to test this idea with data assimilation applied for water temperature. Four cases were considered in the experiment. In case a, three hypothetical moorings were deployed (see Figure 1), one at each entrance or exit. In cases b–d, only a single hypothetical mooring was
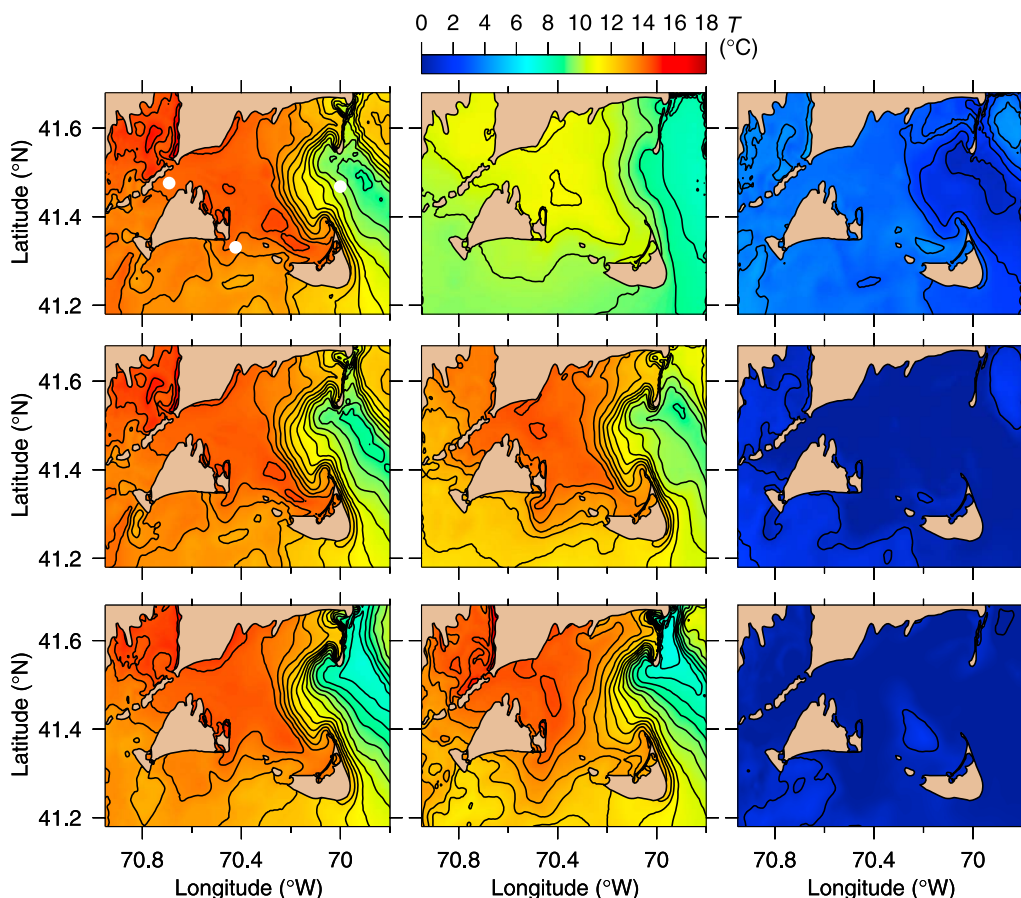
Figure 5. The distributions of (left) the "true" and (middle) analysis surface temperatures and (right) their difference at hours 0, 1, and 12 for case a. White dots in the top left plot are the three sampling sites used for this experiment.

deployed, which was located in the eastern entrance between Cape Cod and Nantucket Island in case b, in the southern entrance between Nantucket Island and Martha's Vineyard Island in case c, and in Vineyard Sound in case d.

[23] In case a, the EnKF succeeded in restoring the model field toward to the true solution within the random error range implemented in the 20 members of ensemble. The root-mean-square (RMS) error of temperature dropped from an initial value of ~3°C to 0.25°C within the first 24 h and remained at this noise level afterward (Figure 5). This result suggests that by assimilating the "observed" temperature at the entrance and exit of Nantucket Sound, the model can restore the temperature field in this region toward the true state. This also means that with the correct surface heat flux, correcting the temperature flux at boundaries of Nantucket Sound through the data assimilation is capable to filter the noise generated by the initial condition in the interior.

[24] The cases b–d were designed to determine which boundary plays a critical role in controlling this system. The EnKF results predict significant convergence tendencies for these three cases (Figure 6). The performance is best in case d and the worst in case b. Case c shows the same convergence rate as case d in the first hour, but the errors do not decrease monotonically as in case d. The RMS error after the first 24 h assimilation period is 1°C for case b; 0.4°C for

case c; and 0.27°C for case d. The results for case d are very similar to that for case a, suggesting that the exit of Nantucket Sound through Vineyard Sound should be considered as the optimal location of temperature measurements if the monitoring system consists of a single mooring in one of the entrances or exits of this region.

[25] To test the sensitivity of sampling locations at each boundary to the assimilation convergence rate, we repeated case b and c experiments by moving the mooring site from location b (shallow) to b_1 (deep) and from location c (deep) to c_1 (shallow), respectively (Figure 1). The results show that the convergence rates are improved when the sampling location is moved to a deeper region. However, case d still produced the fastest convergence rate.

5. Comparisons of Different Optimal Sampling Strategies

[26] A comparison is made here for sampling strategies of EnTKF, POD and Max-Corr via the EnKF result for case d in section 4. Using EnTKF, we found that the location marked by e (hereafter referred to as site e; Figure 1) has the maximum signal variance (Figure 7a). By definition, site e should be an optimal location for the temperature measurement. Selecting this location and assimilating the tem-
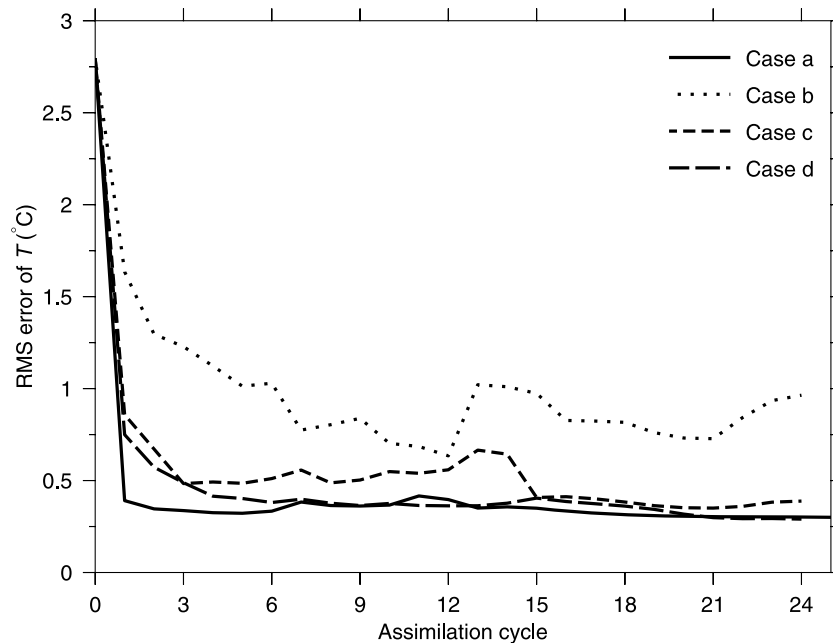
Figure 6. Change of the domain-averaged RMS errors in temperature with time in the first 24 assimilation cycles for cases a, b, c, and d. The assimilation was conducted on an hourly basis.

perature data into the model by EnKF, we found that the RMS error predicted by this method, however, does not show a faster decrease than that for case d, and the RMS error remains over 1°C after 24 hourly assimilation cycles (Figure 8).

[27] Site f is the location of the maximum variance calculated in the EOF analysis of initial ensemble temperature fields following POD (Figure 7b). Through assimilating the temperature data at this site into the model, the model does show a better convergence than the result from the signal variance method using EnTKF. The RMS error sharply drops during the first three assimilation cycles (Figure 8). After a 1 day assimilation, the RMS error decreases to ~0.6°C, however, the convergence rate toward the true state in this case is still not as good as in case d. The determination of the largest variance site in EOF modes depends on the "snapshots" of the water temperature field used to create these modes. Due to the temporal and spatial variation of the coastal system, the largest variation site of the dominant EOF modes of water temperature may differ when different snapshots are taken. The sites f_1 and f_2 are the locations of the largest variation of the first dominant EOF mode created by the model "true" temperature fields for the entire month (sampled over a 3 h interval) and of the first week of that month (sampled over a hourly interval), respectively (Figures 7c and 7d). The convergence tendencies in these two cases are improved in the first three assimilation cycles when compared to the case with site f, but the RMS errors after six assimilation cycles for all three cases remains similar (Figure 8).

[28] Site g is the location at which $\bar{S}$ is a maximum (Figure 7e). Selecting this point as the observation site, the assimilation shows a fast convergence almost the same as that shown in case d. The RMS error drops quickly in the first assimilation cycle, down to ~0.5°C by the fifth assimilation cycle, and then remains at a value of ~0.35°C after

that (Figure 8). The Max-Corr method was inspired by the traditional Kalman filter formulation, which shows that the influence function $P^f H^T$ spreads the observational information to the entire assimilation region. This suggests that the average correlation between the observation and entire domain becomes important for the success of Kalman filters. One could imagine that if the selected observation site has no or low correlation with the rest of the assimilation domain, the model would be unable to make an accurate estimate of model state based on information from this sampling location.

6. Lagrangian Particle- and Tracer-Tracking Experiments

[29] The OSSEs results show that the convergence rates of placing sensor location by seeking maximum signal variance (EnTKF) or by seeking extrema of dominant EOF modes (POD) are not as good as sampling at site d in Vineyard Sound and site g determined by the Max-Corr method. To explain why the assimilation results are sensitive to location, we conducted particle- and tracer-tracking experiments to examine the flow field in Nantucket Sound.

[30] A total of 92 particles (~30 particles at each transect) were released at the eastern, southern and western boundaries of Nantucket Sound at the beginning of June 2006 and tracked for 7 days, respectively (Figure 9). The subtidal trajectories show that the particles released at the eastern boundary all flowed southward out of Nantucket Sound and then around Nantucket Island to continue moving westward, with a few particles entering the southern boundary of Nantucket Sound. This suggests that during the assimilation period, the water inside Nantucket Sound was not supplied from the eastern boundary, which explains why the convergence rate was low when the sampling location was placed at that boundary. The subtidal particle trajectories
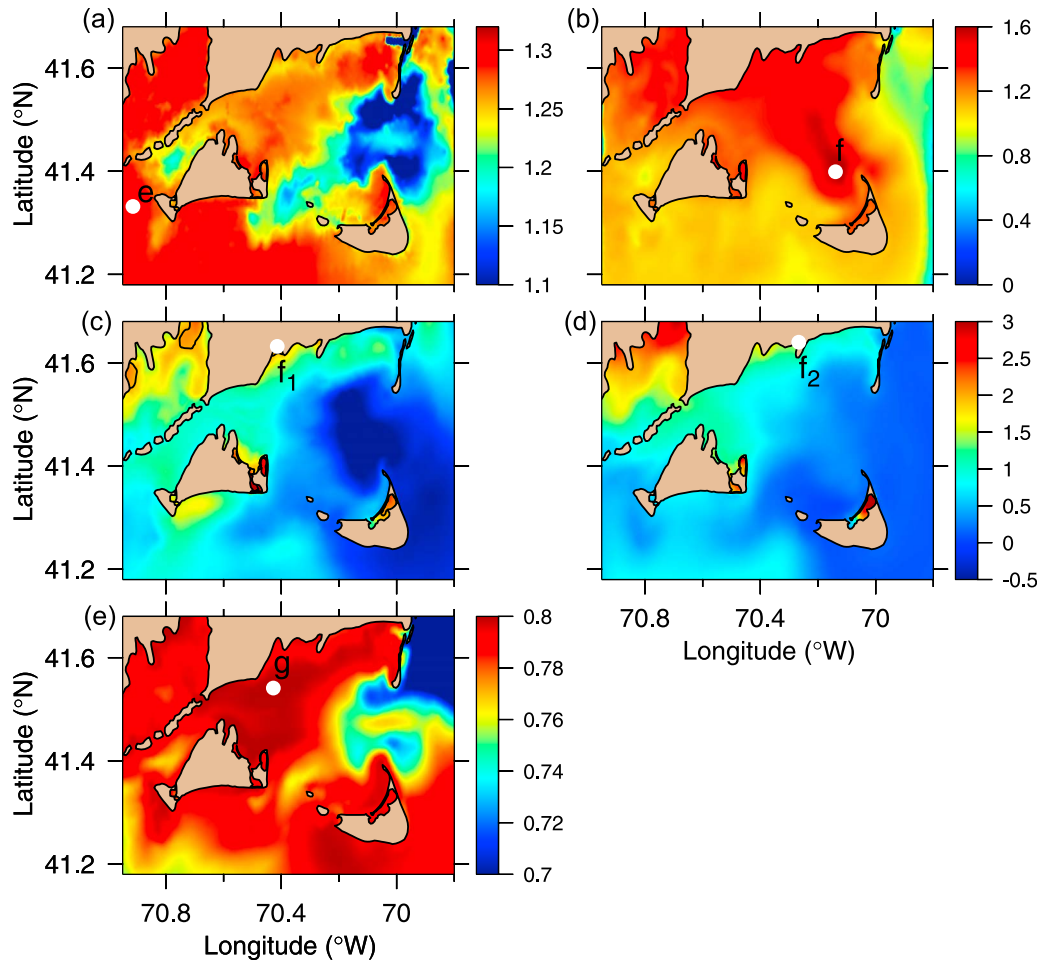
Figure 7. (a) Distribution of the signal variance estimated by EnTKF, with "e" showing the location of the maximum signal variance. Distributions of the first dominant POD spatial modes of the temperature calculated using the initial ensemble and the true model field sampled at (b) hourly intervals in the first week of June and (c) a 3 h interval in the entire period of June; f, f_1 and f_2 are the locations of the largest variation of the first mode for these three cases, respectively. (e) Distributions of correlation coefficients calculated using the initial ensemble, with "g" showing the location of the maximum correlation value.
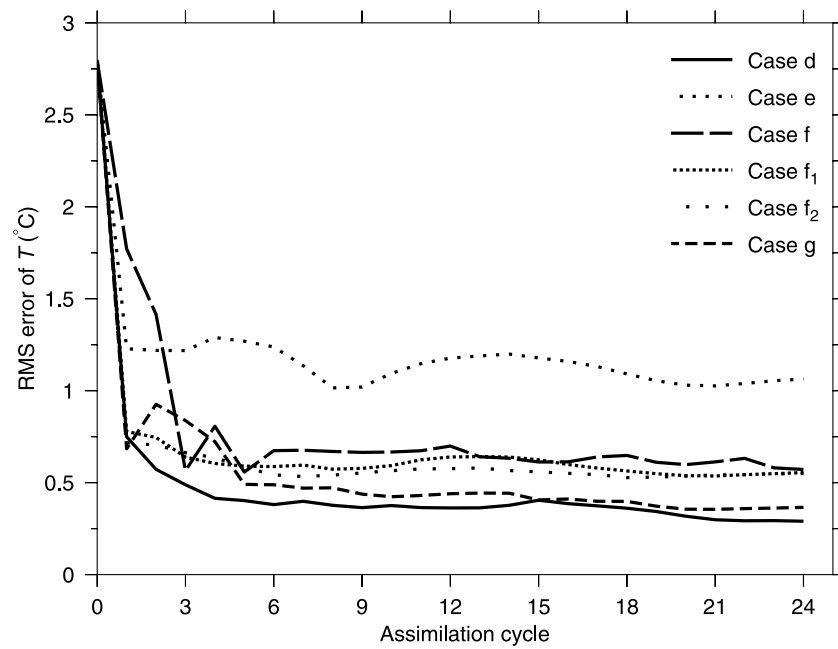
Figure 8. Comparison of the domain-averaged RMS errors of temperatures estimated for case d with those estimated for cases e, f, f_1, f_2, and g.
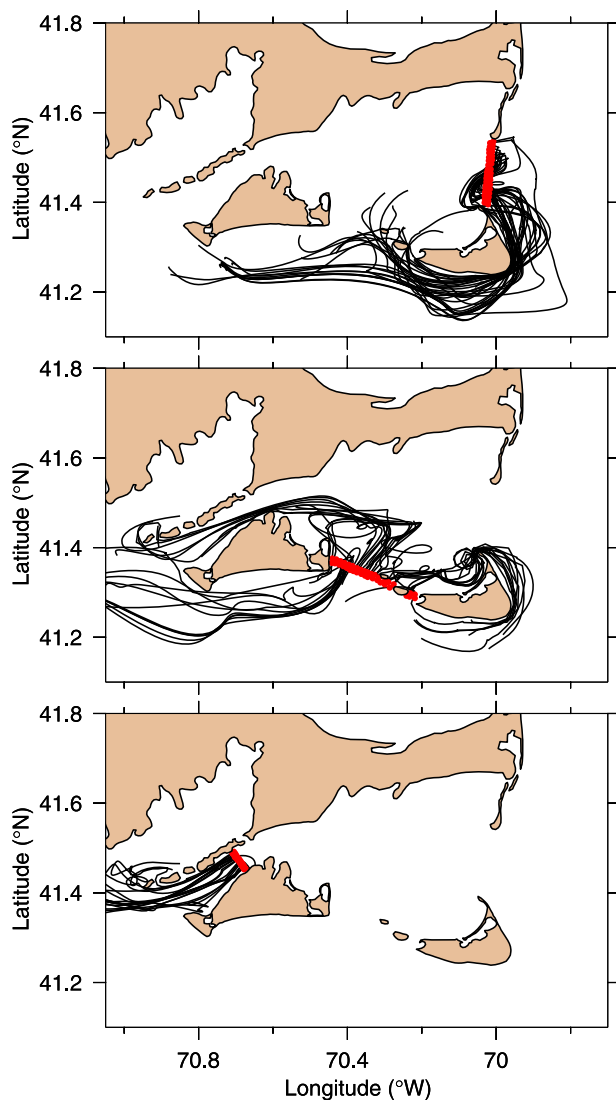
Figure 9. Subtidal particle trajectories released at the (top) eastern, (middle) southern, and (bottom) western boundaries of Nantucket Sound at the beginning of June and tracked for 7 days. Red lines indicate the three transects where particles were released. The total number of particles released was 92 (~30 particles at each transect).

released at the southern boundary show three major paths: the first flowing northeastward and then turning westward to flow through Vineyard Sound, the second moving southwestward around Martha's Vineyard Island toward Buzzards Bay, and the third drifting northeastward around Nantucket Island. It is clear that the first path is the major inflow water source to the interior of Nantucket Sound, while the third path features a local around-the-island flow and second path represented a local cyclonic return flow around Martha's Vineyard Island. This explains why the assimilation results at a sampling site in the first path of the water stream shows a better convergence rate than that at the eastern boundary, because the flow in the interior of Nantucket Sound is controlled by the inflow from that area. All particles released at the upstream area of Vineyard Sound flowed southwestward along the sound toward

Rhode Island Sound and Buzzards Bay. Water in the interior of Nantucket Sound clearly flows out through its western exit into Vineyard Sound, thus any change in the water transport in Vineyard Sound directly affects the flow in the interior of Nantucket Sound. This is the reason why placing the sampling site in Vineyard Sound shows the best convergence rate in the assimilation experiments (case d).

[31] The same features were found in the tracer-tracking experiments. *Chen et al.* [2008] pointed out that in an inhomogeneous flow field, tracer movement significantly differs from particle movement due to vertical and lateral diffusion. Dyes with a unit concentration were injected throughout the water column at the eastern and southern boundaries and the interior region of Nantucket Sound (see the white bars and white box in Figure 10), respectively. The resulting spread of the dye released on the eastern and southern boundaries was consistent with the particle trajectories. At the eastern boundary, the core of the dye moved southward and then around Nantucket Island, while a small portion entered Nantucket Sound and then flowed northward within the near-boundary region of roughly 20 km, the local tidal excursion scale. This suggests that the motion around the eastern boundary features two distinct local scales (wind and tide-induced flows), with little direct correlation to the outflow in Nantucket Sound. Similarly at the southern boundary, the flow features two distinct scales: one is for the regional scale directly related to the motion in the interior of Nantucket Sound and outflow in Vineyard Sound, and the other is for the local scale related to the flow around Martha's Vineyard Island and Nantucket Island. The dye released in the interior of Nantucket Sound mostly flowed toward Vineyard Sound, with a small portion flowing out of Nantucket Sound at the eastern and southern boundaries.

[32] Both particle- and dye-tracking results suggest that the flow in Nantucket Sound is controlled by multiscale physical processes: local tidal forcing, local and island-related topographic interactions, and larger-scale subtidal wind and buoyancy forcing. Figure 11 shows the tidal excursion scale in Nantucket Sound. In the interior, the scale is about 10~15 km; at each boundary, the maximum is over 25 km. The complex features of the currents are seen in the distribution of monthly averaged near-surface subtidal currents shown in Figure 12. Figure 12 clearly shows the multiscale flow field characterized by tidal flushing-induced eddies, slow subtidal flow and large horizontal current shears. For the regional scale, Nantucket Sound is a "flow-through" system, but on a local scale, it is a tidally flushed and geometrically controlled system. For a given surface net heat flux, temperature in Nantucket Sound is controlled primarily by advection through the boundaries. Thus if the monitoring is aimed at forecasting water temperature in the interior of Nantucket Sound, the sampling plan should be designed to reflect the regional-scale "flow-through" system.

7. Conclusions

[33] OSSEs were conducted for Nantucket Sound to investigate different approaches to design an optimal monitoring system in this region. Experiments were carried out using the local higher-resolution Nantucket Sound subdomain FVCOM model through nesting with the regional
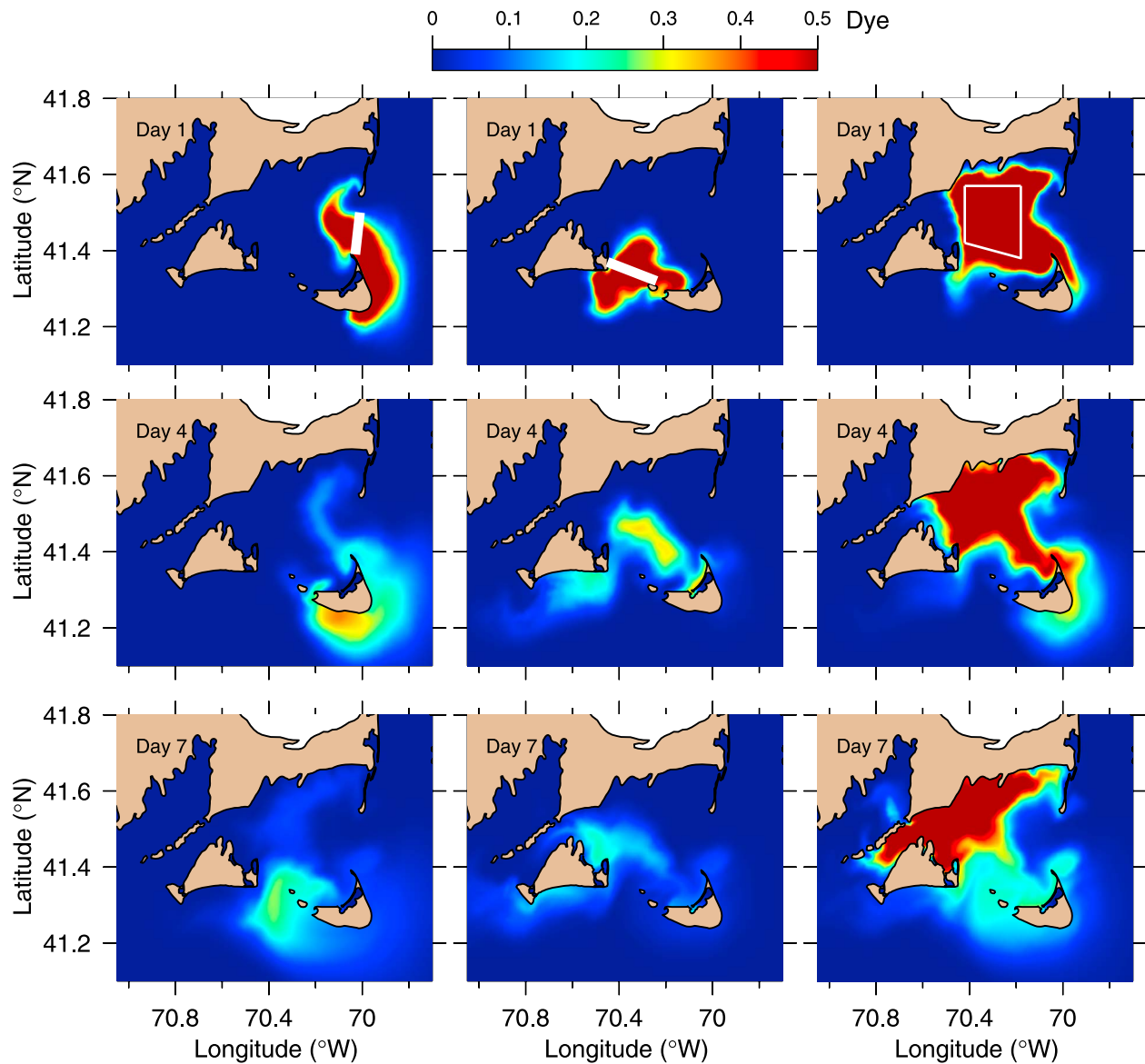
Figure 10. Distributions of the vertically averaged dye concentrations at (top) day 1, (middle) day 4, and (bottom) day 7 for the cases in which dye was injected throughout the water column at the (left) eastern and (middle) southern boundaries and (right) the interior region of Nantucket Sound. The white bars and the area enclosed by the white box indicate the regions of initial dye injection.
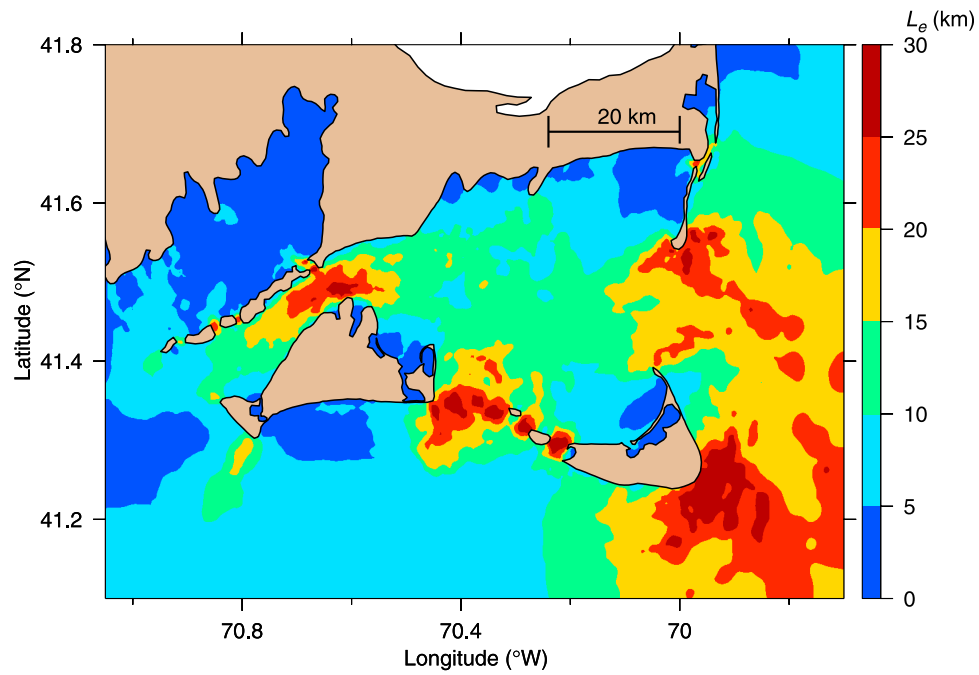
Figure 11. Map of tidal excursion scale (L_θ) in Nantucket Sound and adjacent region estimated using the model simulation results.
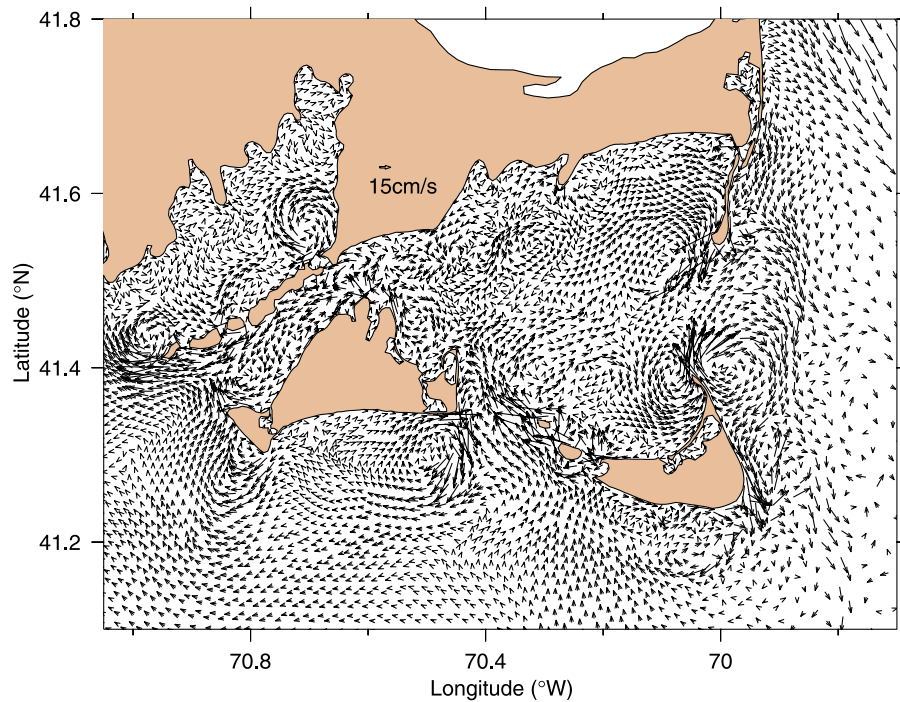
Figure 12. The FVCOM-predicted monthly averaged subtidal surface currents for June 2006.
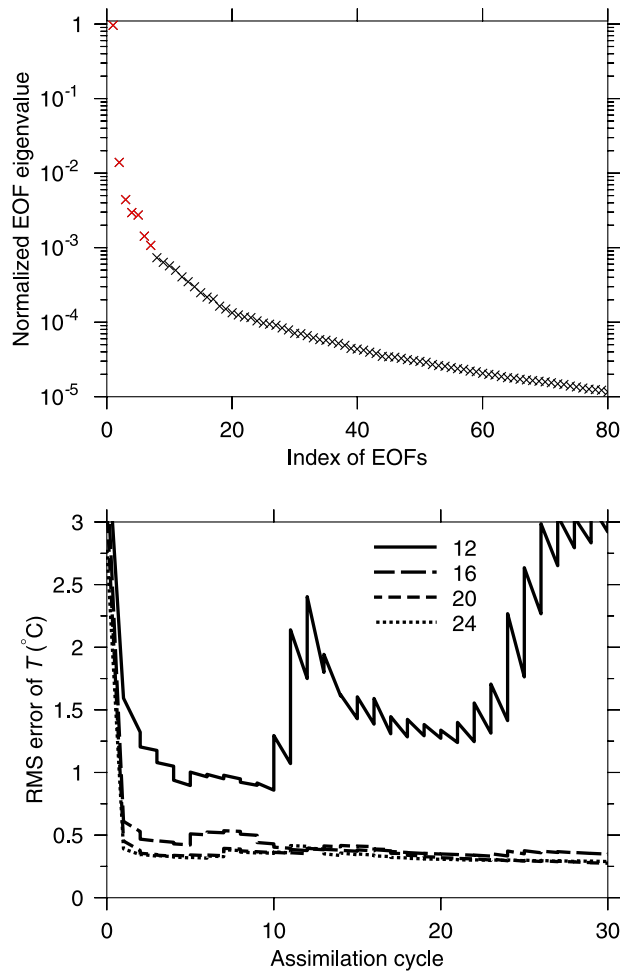
Figure A1. (top) The first 80 normalized EOF eigenvalues calculated using the temperature field output at a 3 h interval from the simulation ("true state") experiment. (bottom) Changes in the domain-averaged RMS temperature errors during the first 30 EnKF assimilation cycles for the cases with an ensemble size $N = 12$, 16, 20, and 24.

FVCOM-GOM2. The results suggest that in this vertically well-mixed coastal region, the velocity and surface elevation have a self-restoring nature over an inertial period scale after initial perturbation, while water temperature and salinity do not. By placing temperature measurement sites at the open boundaries of this "flow-through" system, the assimilation results show that locating the sampling site at the exit of Nantucket Sound into Vineyard Sound produces better convergence than when the site is located on the eastern and southern boundaries. Lagrangian and tracer-tracking experiments show that the flow in Vineyard Sound is directly correlated with the flow in the interior of Nantucket Sound, while the flows around the eastern and southern boundaries are characterized by multiscale processes with much lower correlation with the interior Nantucket Sound flow. The sampling locations determined by the maximum signal variance suggested by EnTKF or the extrema of spatial EOF modes suggested by POD do not provide as good a result as the sampling sites located in Vineyard Sound. These results indicate that attention should be paid to the multiscale nature of physical processes in the

study region when an assimilation method is used to design the optimal monitoring network.

[34] By constructing a preconditional ensemble using dominant modes, SEIK can significantly reduce the requirement of a large ensemble size and thus improve the Kalman filter data assimilation in comparison with EnKF. This method is suitable for OSSEs in the coastal ocean.

[35] Our OSSEs in Nantucket Sound were conducted as a pilot study for the coastal region. Since the dynamics in the coastal ocean vary significantly in time and space, the results found in this system may not be applicable to other coastal regions. The most important result of this work is the approach used in the design of the optimal monitoring sites. Designing the monitoring network should be undertaken with a full understanding of the multiscale dynamical nature of the study area, rather than depend solely on data assimilation methods.

Appendix A: Comparisons of EnKF and SEIK for Optimization of Ensemble Generation

[36] The OSSEs conducted with EnKF in this study provide us with a tool to design and evaluate the optimal design of a sampling plan in Nantucket Sound. In most real applications, however, one of major concerns in using EnKF is how to create the initial ensemble with an appropriate size that can capture the main characteristics of the true error covariance. Since the computational time required for the assimilation is proportional to the size of the ensemble, it becomes impractical to use EnKF for the forecast operation if a large ensemble size is required.

[37] SEIK is the ensemble Kalman filter method with a different strategy of creating the initial ensemble. In traditional Monte Carlo sampling, in order to let the ensemble-represented error covariance converge to the true error covariance, one usually tries to include more model states in the ensemble [*Hamill et al.*, 2001; *Evensen*, 2004]. As long as the additional model states increase the spanned error subspace, this approach leads to a more accurate estimation of true error covariance but scarifies at a proportional increase in computational effort. Alternatively, *Nerger et al.* [2005] showed that the ensemble size can be reduced by using the initialization approach proposed with SEIK [*Pham et al.*, 1998]. By preanalyzing a large amount of model states and rotating them to generate preconditioned initial states that retain the span of error subspace in the smaller ensemble size, SEIK can achieve the same assimilation results with a significantly smaller ensemble size. In theory, the minimum ensemble size can be the dominant error covariance rank plus one [*Pham et al.*, 1998; *Nerger et al.*, 2005]. An ensemble generation procedure analogous to that typically used in SEIK for the EnKF was discussed by *Evensen* [2004].

[38] In this study, we tested SEIK with a comparison to EnKF. Two experiments were made. In the first experiment, we tested EnKF by selecting different ensemble sizes. This experiment was aimed to determine the minimum ensemble size for EnKF for this dynamical system. Then in the second experiment, we conducted SEIK to determine the efficiency of this approach in reducing the ensemble size via EnKF.

[39] In the first experiment, to determine the ensemble size for our data assimilation experiment, we first sampled
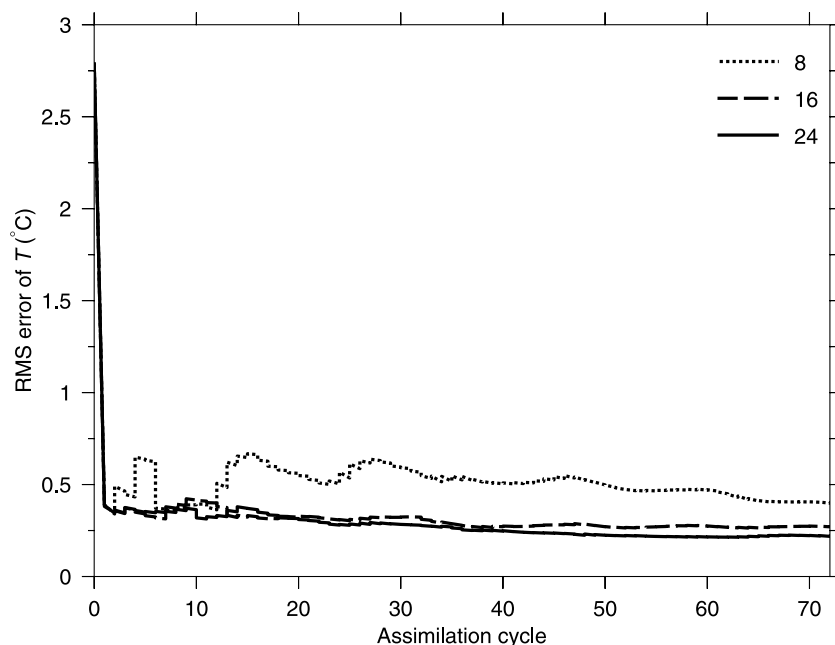
Figure A2. Changes in the domain-averaged RMS temperature errors during the first 72 assimilation cycles for the SEIK experiments with an ensemble size $N = 8$, 16, and 24.

240 model states with a 3 h interval over the entire month of June. Figure A1 (top) shows the normalized EOF eigenvalues. The first seven eigenvalues represented over 99% of the total energy captured by the 240 model states. It indicates that Nantucket Sound can be described as a low-dimensional system (which was pointed out in the POD experiment by *Yang et al.* [2011]). For this reason, we expect that the required ensemble size is O(10). We reran EnKF with an ensemble size $N = 8$, 12, 16, 20 and 24; results are shown in Figure A1 (bottom). For $N = 8$, EnKF failed to produce a convergence solution (not shown). For $N = 12$, EnKF converged for a few assimilation cycles before diverging in later stages. With $N = 16$, the filter showed a good and stable performance and the RMS error dropped to 0.32°C over the first 30 h (0.25°C over the 96 h) assimilation cycles. No significant improvement was found for N = 20 and 24, indicating that 16 member ensemble were sufficient for EnKF in the Nantucket Sound OSSEs, although for a conservative approach, we used ensemble with $N = 20$ in our experiments presented in this study.

[40] In the second experiment, following *Nerger et al.* [2005], we used the computational efficient analysis formulation to construct a preconditional ensemble for SEIK. The basic idea of this formulation is to generate the stochastic ensemble of $r + 1$ state initialization to represent the r largest eigenmodes (which usually (but not necessarily) can be done with EOFs) of the predetermined error covariance through the larger presampling of the initial state. This approach allows a model to describe the error covariance with a minimum ensemble size while the error evolution is still propagated by the nonlinear model as the EnKF. A detailed description of this method was given by *Pham et al.* [1998] and *Nerger et al.* [2005].

[41] We presampled 24 model initial states to estimate the initial error covariance. With SEIK, we generated 8, 16, 20 and 24 preconditioned ensemble members based on the

largest 7, 15, 19 and 23 eigenmodes, respectively. In our EOF analysis for the first experiment, the dominant 7 eigenmodes account for over 99% of the total energy in the estimated error covariance. The assimilation results of SEIK show that with an ensemble size $N = 8$, SEIK was able to produce as good a performance as was obtained with EnKF with $N = 16$, with a reduction of the computation load of EnKF nearly 50% (Figure A2). Nonetheless, a larger ensemble size with SEIK also shows a better and more stable performance (Figure A2). It is clear that a larger ensemble size acts to restrain the noise-to-signal ratio. For real coastal applications, SEIK should be more computationally efficient than EnKF.

References

Ballabrera-Poy, J., E. Hackert, R. Murtugudde, and A. J. Busalacchi (2007), An observing system simulation experiment for an optimal

moored instrument array in the tropical Indian Ocean, *J. Clim.*, *20*, 3284–3299, doi:10.1175/JCLI4149.1.

Bishop, C. H., B. J. Etherton, and S. J. Majumdar (2001), Adaptive sampling with the ensemble transform Kalman filter. Part I: Theoretical aspects, *Mon. Weather Rev.*, *129*, 420–436, doi:10.1175/1520-0493 (2001)129<0420:ASWTET>2.0.CO;2.

Charney, J., M. Halem, and R. Jastrow (1969), Use of incomplete historical data to infer the present state of the atmosphere, *J. Atmos. Sci.*, *26*, 1160–1163, doi:10.1175/1520-0469(1969)026<1160:UOIHDT>2.0. CO;2.

Chen, C., H. Liu, and R. C. Beardsley (2003), An unstructured grid, finite-volume, three-dimensional, primitive equations ocean model: Application to coastal ocean and estuaries, *J. Atmos. Oceanic Technol.*, *20*(1), 159–186, doi:10.1175/1520-0426(2003)020<0159:AUGFVT>2.0.CO;2.

Chen, C., R. C. Beardsley, and G. Cowles (2006a), An unstructured grid, finite-volume coastal ocean model (FVCOM) system, *Oceanography*, *19*(1), 78–89.

Chen, C., R. C. Beardsley, and G. Cowles (2006b), An unstructured grid, finite-volume coastal ocean model: FVCOM user manual, 2nd ed., *Tech. Rep. SMAST/UMASSD-06-0602*, 315 pp., Sch. for Mar. Sci. and Technol., Univ. of Mass. at Dartmouth, Dartmouth.

Chen, C., Q. Xu, R. Houghton, and R. C. Beardsley (2008), A model-dye comparison experiment in the tidal mixing front zone on the southern flank of Georges Bank, *J. Geophys. Res.*, *113*, C02005, doi:10.1029/ 2007JC004106.

Chen, C., P. Malanotte-Rizzoli, J. Wei, R. C. Beardsley, Z. Lai, P. Xue, S. Lyu, Q. Xu, J. Qi, and G. W. Cowles (2009), Application and comparison of Kalman filters for coastal ocean problems: An experiment with FVCOM, *J. Geophys. Res.*, *114*, C05011, doi:10.1029/2007JC004548.

Evensen, G. (1994), Sequential data assimilation with a nonlinear quasi-geostrophic model using Monte Carlo methods to forecast error statistics, *J. Geophys. Res.*, *99*(C5), 10,143–10,162, doi:10.1029/94JC00572.

Evensen, G. (2003), The ensemble Kalman filter: Theoretical formulation and practical implementation, *Ocean Dyn.*, *53*(4), 343–367, doi:10.1007/s10236-003-0036-9.

Evensen, G. (2004), Sampling strategies and square root analysis schemes for the EnKF, *Ocean Dyn.*, *54*(6), 539–560, doi:10.1007/s10236-004-0099-2.

Hackert, E., R. Miller, and A. Busalacchi (1998), An optimized design for a moored instrument array in the tropical Atlantic Ocean, *J. Geophys. Res.*, *103*(C4), 7491–7509, doi:10.1029/97JC03206.

Hamill, T. M., J. S. Whitaker, and C. Snyder (2001), Distance-dependent filtering of background error covariance estimates in an ensemble Kalman filter, *Mon. Weather Rev.*, *129*, 2776–2790, doi:10.1175/1520-0493(2001)129<2776:DDFOBE>2.0.CO;2.

Intergovernmental Oceanographic Commission (2003), The integrated strategic design plan for the coastal ocean observations module of the Global Ocean Observing System, *GOOS Rep. 125*, U. N. Educ., Sci., and Cult. Organ., Paris.

Majumdar, S. J., C. H. Bishop, B. J. Etherton, and Z. Toth (2002), Adaptive sampling with the ensemble transform Kalman filter. Part II: Field program implementation, *Mon. Weather Rev.*, *130*, 1356–1369, doi:10.1175/1520-0493(2002)130<1356:ASWTET>2.0.CO;2.

Nerger, L., W. Hiller, and J. Schröter (2005), A comparison of error subspace Kalman filters, *Tellus, Ser. A*, *57*(5), 715–735, doi:10.1111/ j.1600-0870.2005.00141.x.

Pham, D. T. (2001), Stochastic methods for sequential data assimilation in strongly nonlinear systems, *Mon. Weather Rev.*, *129*, 1194–1207, doi:10.1175/1520-0493(2001)129<1194:SMFSDA>2.0.CO;2.

Pham, D. T., J. Verron, and L. Gourdeau (1998), Singular evolutive Kalman filters for data assimilation in oceanography, *C. R. Acad. Sci., Ser. II*, *326*(4), 255–260.

Pietrzak, J., J. B. Jakobson, H. Burchard, H. J. Vested, and O. Petersen (2002), A three-dimensional hydrostatic model for coastal and ocean modeling using a generalized topography following co-ordinate system, *Ocean Modell.*, *4*(2), 173–205, doi:10.1016/S1463-5003(01)00016-6.

Raicich, F., and A. Rampazzo (2003), Observing system simulation experiments for the assessment of temperature sampling strategies in the Mediterranean Sea, *Ann. Geophys.*, *21*, 151–165, doi:10.5194/ angeo-21-151-2003.

Willcox, K. (2006), Unsteady flow sensing and estimation via the gappy proper orthogonal decomposition, *Comput. Fluids*, *35*(2), 208–226, doi:10.1016/j.compfluid.2004.11.006.

Yang, X., D. Venturi, C. Chen, C. Chryssostomidis, and G. E. Karniadakis (2011), EOF-based constrained sensor placement and field reconstruction from noisy ocean measurements: Application to Nantucket Sound, *J. Geophys. Res.*, *116*, C12072, doi:10.1029/2010JC006148.

Yildirim, B., C. Chryssostomidis, and G. E. Karniadakis (2009), Efficient sensor placement for ocean measurements using low-dimensional concepts, *Ocean Modell.*, *27*(3–4), 160–173, doi:10.1016/j.ocemod. 2009.01.001.

R. C. Beardsley and R. Limeburner, Department of Physical Oceanography, Woods Hole Oceanographic Institution, Woods Hole, MA 02543, USA.

C. Chen and P. Xue, School for Marine Science and Technology, University of Massachusetts Dartmouth, New Bedford, MA 02744, USA. (pxue@umassd.edu)